International Forum on Aeroelasticity and Structural Dynamics
IFASD 2017
25-28 June 2017 Como, Italy

APPLICATION OF NONLINEAR MODEL ORDER REDUCTION TECHNIQUE TO A FLEXIBLE AIRCRAFT FOR REAL-TIME SIMULATIONS

Juliano A. Paulino[1], Flávio J. Silvestre[1], Antônio B. Guimarães Neto[1], Tiago P. Monteiro[1], Roberto Gil A. da Silva[1], Andrea Da Ronch[2]

[1]Divisão de Engenharia Aeronáutica
Instituto Tecnológico de Aeronáutica
São José dos Campos, SP, 12228-900, Brazil
paulino.juliano@gmail.com
flaviojs@ita.br
antoniobgn@gmail.com
tiago.priolli@gmail.com
gil@ita.br

[2]Engineering and the Environment
University of Southampton
Southampton, SO171BJ, UK
A.Da–Ronch@soton.ac.uk

Keywords: real–time simulation, reduced-order modeling, flexible aircraft, flight dynamics, aeroelasticity

Abstract: Real–time simulation is a valuable tool for aircraft development. However, flexible aircraft models are computationally expensive and can be prohibitive for fast simulations. This paper investigates the applicability of a nonlinear model order reduction technique to a moderate flexible aircraft for real–time simulation purposes. Details of the implementation and test cases are presented. Results show that the reduced–order model can be simulated in real–time and produces better results than linearized model and rigid–body model with aeroelastic correction and we conclude that the technique is promising for real–time simulations.

1 INTRODUCTION

Real–time flight simulation is a valuable tool for aircraft development. The benefits are beyond design. Financial costs can be reduced and development process can be accelerated by using flight simulators instead of flying prototypes. Furthermore, safety can be increased by providing pilots ground training, reconstructing flight conditions involved in accidents or simulating abnormal situations that could be dangerous to be reproduced in real flight.

Because of the benefits, real–time flight simulation models are widely used by industry and academic research. They are fundamental part of hardware–in–the–loop (HIL) and pilot–in–the–loop (PIL) simulations and have plenty of applications. For example, HIL simulations can be used to validate control systems [1, 2] and PIL simulations can be used to evaluate flying qualities [3] or for pilot induced oscillations (PIO) studies [4].

However, real–time flight simulation for flexible aircraft is currently a challenge. The interaction between fluid, structure and flight dynamics results in mathematical models with many state variables and highly nonlinear equations, which are computationally expensive to be calculated in real–time. In addition, linear models cannot represent the aeroelastic effects accurately when large aircraft body deformation or large angles of incidence are involved.

In face of these difficulties, new simulation strategies must be studied. This work investigates the applicability of a nonlinear model order reduction technique [5] for real–time simulation purposes. The technique is applied to a moderate flexibility aircraft model, the Generic Narrow Body Airliner (GNBA) in its most flexible configuration (W025F025) [6] and the results are compared with fast simulation approaches: the classical rigid–body approximation with quasi–steady aeroelastic correction and the linearized full–order flexible model.

2 THE MODEL ORDER REDUCTION TECHNIQUE

The nonlinear model order reduction technique employed in the current work was developed by Da Ronch et al [5]. It was conceived for flight control law design of flexible aircraft. In summary, the technique uses information on the eigenspectrum of the Jacobian matrix and projects the system through a Taylor series expansion onto a small basis of eigenvectors representative of the system dynamics, retaining terms of second and third order.

Consider a flexible aircraft with dynamics represented by the state equation

$$\dot{\boldsymbol{x}} = \boldsymbol{F}(\boldsymbol{x}, \boldsymbol{u}), \tag{1}$$

where $\boldsymbol{F}$ is a nonlinear function, $\boldsymbol{u}$ is the control input vector and $\boldsymbol{x}$ is a n–dimensional state vector containing rigid–body, structural and fluid state variables:

$$\boldsymbol{x} = \begin{bmatrix} \boldsymbol{x_{rb}} \\ \boldsymbol{x_s} \\ \boldsymbol{x_f} \end{bmatrix}_{n\times 1}. \tag{2}$$

Consider now $\boldsymbol{\Delta x} = \boldsymbol{x} - \boldsymbol{x_0}$ a small perturbation in the state vector with respect to an equilibrium point $\boldsymbol{x_0}$ and $\boldsymbol{\Delta u} = \boldsymbol{u} - \boldsymbol{u_0}$ a small perturbation in the control input vector with respect to the equilibrium point $\boldsymbol{u_0}$. The nonlinear state equation represented by Eq. (1) is expanded in a Taylor series around $\boldsymbol{x_0}$ and $\boldsymbol{u_0}$ and the system dynamics is approximated by

$$\boldsymbol{\Delta \dot{x}} \approx \boldsymbol{A\Delta x} + \frac{\partial \boldsymbol{F}}{\partial \boldsymbol{u}}\boldsymbol{\Delta u} + \frac{1}{2!}\boldsymbol{B}(\boldsymbol{\Delta x}, \boldsymbol{\Delta x}) + \frac{1}{3!}\boldsymbol{C}(\boldsymbol{\Delta x}, \boldsymbol{\Delta x}, \boldsymbol{\Delta x}), \tag{3}$$

where $\boldsymbol{A}$, $\boldsymbol{B}$ and $\boldsymbol{C}$ represents the first, second and third Jacobian operators defined by

$$A_{ij} = \frac{\partial F_i(\boldsymbol{x_0})}{\partial x_j}, \tag{4}$$

$$B_i(\boldsymbol{a}, \boldsymbol{b}) = \sum_{j,k=1}^{n} \frac{\partial^2 F_i(\boldsymbol{x_0})}{\partial x_j \partial x_k} a_j b_k, \tag{5}$$

$$C_i(\boldsymbol{a}, \boldsymbol{b}, \boldsymbol{c}) = \sum_{j,k,l=1}^{n} \frac{\partial^3 F_i(\boldsymbol{x_0})}{\partial x_j \partial x_k \partial x_l} a_j b_k c_l. \tag{6}$$

The Taylor series expansion (3) must be projected onto a small basis formed by m ($m \ll n$) eigenvectors of the Jacobian matrix $\boldsymbol{A}$ which are representative of the aircraft dynamics. Denote $\boldsymbol{\phi_i}$ and $\boldsymbol{\psi_i}$ the right and left eigenvectors of $\boldsymbol{A}$, i.e.

$$\boldsymbol{A\phi_i} = \lambda_i \boldsymbol{\phi_i}, \quad \text{for } i = 1, ..., n, \tag{7}$$

$$\boldsymbol{A}^T \boldsymbol{\psi_i} = \bar{\lambda}_i \boldsymbol{\psi_i}, \quad \text{for } i = 1, ..., n. \tag{8}$$

It is convenient that the set of eigenvectors that forms the reduced–order model basis satisfies the biorthonormality conditions, i.e.

$$\langle \boldsymbol{\phi_i}, \boldsymbol{\phi_i} \rangle = 1, \quad \text{for } i = 1, ..., m, \tag{9}$$

$$\langle \boldsymbol{\psi_j}, \boldsymbol{\phi_i} \rangle = \delta_{ij}, \quad \text{for } i = 1, ..., m, \tag{10}$$

$$\langle \boldsymbol{\psi_j}, \bar{\boldsymbol{\phi}}_i \rangle = 0, \quad \text{for } i = 1, ..., m, \tag{11}$$

where δ_{ij} represents the Kronecker delta and the inner product is defined as $\langle \boldsymbol{a}, \boldsymbol{b} \rangle = \bar{\boldsymbol{a}}^T \boldsymbol{b}$.

Consider the transformation of coordinates

$$\boldsymbol{\Delta x} = \boldsymbol{\Phi z} + \bar{\boldsymbol{\Phi}} \bar{\boldsymbol{z}}, \tag{12}$$

where

$$\boldsymbol{\Phi} = \begin{bmatrix} \boldsymbol{\phi_1} & \boldsymbol{...} & \boldsymbol{\phi_m} \end{bmatrix} \tag{13}$$

and $\boldsymbol{z} \in \mathbb{C}^m$ is the reduced–order model state variable vector. Applying the transformation of coordinates (12) into Eq. (3) and then premultiplying each term by the conjugate transpose of of the left modal matrix, results in

$$\bar{\boldsymbol{\psi}}_j^T (\boldsymbol{\phi_i} \dot{z}_i + \bar{\boldsymbol{\phi}}_i \dot{\bar{z}}_i) = \bar{\boldsymbol{\psi}}_j^T \Big(\boldsymbol{A\phi_i} z_i + \boldsymbol{A}\bar{\boldsymbol{\phi}}_i \bar{z}_i + \frac{\partial \boldsymbol{F}}{\partial \boldsymbol{u}} \boldsymbol{\Delta u} + \frac{1}{2!} B_i(\boldsymbol{\Delta z}, \boldsymbol{\Delta z}) + \frac{1}{3!} C_i(\boldsymbol{\Delta z}, \boldsymbol{\Delta z}, \boldsymbol{\Delta z}) \Big). \tag{14}$$

Once the biorthonormality conditions (9), (10) and (11) were satisfied, the set of m equations (14) can be simplified as

$$\dot{z}_i = \lambda_i z_i + \boldsymbol{\psi}_j^T \Big(\frac{\partial \boldsymbol{F}}{\partial u} \boldsymbol{\Delta u} + \frac{1}{2!} B_i(\boldsymbol{\Delta z}, \boldsymbol{\Delta z}) + \frac{1}{3!} C_i(\boldsymbol{\Delta z}, \boldsymbol{\Delta z}, \boldsymbol{\Delta z}) \Big), \tag{15}$$

where the bilinear and trilinear terms are written as

$$\begin{aligned} B_i(\boldsymbol{\Delta z}, \boldsymbol{\Delta z}) = \sum_{r,s=1}^{m} & B_i(\boldsymbol{\phi_r}, \boldsymbol{\phi_s}) z_r z_s + B_i(\boldsymbol{\phi_r}, \bar{\boldsymbol{\phi}}_{\boldsymbol{s}}) z_r \bar{z}_s + \\ & B_i(\bar{\boldsymbol{\phi}}_{\boldsymbol{r}}, \boldsymbol{\phi_s}) \bar{z}_r z_s + B_i(\bar{\boldsymbol{\phi}}_{\boldsymbol{r}}, \bar{\boldsymbol{\phi}}_{\boldsymbol{s}}) \bar{z}_r \bar{z}_s \end{aligned} \tag{16}$$

and

$$\begin{aligned} C_i(\boldsymbol{\Delta z}, \boldsymbol{\Delta z}, \boldsymbol{\Delta z}) = \sum_{r,s,t=1}^{m} \Big(& C_i(\boldsymbol{\phi_r}, \boldsymbol{\phi_s}, \boldsymbol{\phi_t}) z_r z_s z_t + C_i(\boldsymbol{\phi_r}, \boldsymbol{\phi_s}, \bar{\boldsymbol{\phi}}_{\boldsymbol{t}}) z_r z_s \bar{z}_t + \\ & C_i(\boldsymbol{\phi_r}, \bar{\boldsymbol{\phi}}_{\boldsymbol{s}}, \boldsymbol{\phi_t}) z_r \bar{z}_s z_t + C_i(\boldsymbol{\phi_r}, \bar{\boldsymbol{\phi}}_{\boldsymbol{s}}, \bar{\boldsymbol{\phi}}_{\boldsymbol{t}}) z_r \bar{z}_s \bar{z}_t + \\ & C_i(\bar{\boldsymbol{\phi}}_{\boldsymbol{r}}, \boldsymbol{\phi_s}, \boldsymbol{\phi_t}) \bar{z}_r z_s z_t + C_i(\bar{\boldsymbol{\phi}}_{\boldsymbol{r}}, \boldsymbol{\phi_s}, \bar{\boldsymbol{\phi}}_{\boldsymbol{t}}) \bar{z}_r z_s \bar{z}_t + \\ & C_i(\bar{\boldsymbol{\phi}}_{\boldsymbol{r}}, \bar{\boldsymbol{\phi}}_{\boldsymbol{s}}, \boldsymbol{\phi_t}) \bar{z}_r \bar{z}_s z_t + C_i(\bar{\boldsymbol{\phi}}_{\boldsymbol{r}}, \bar{\boldsymbol{\phi}}_{\boldsymbol{s}}, \bar{\boldsymbol{\phi}}_{\boldsymbol{t}}) \bar{z}_r \bar{z}_s \bar{z}_t \Big) \end{aligned} \tag{17}$$

It is possible to calculate all the bilinear and trilinear contributions without calculating all the second and third order partial derivatives analytically. They can be approximated by using finite differences instead. The bilinear and trilinear contributions consist, in general, of $4m^2$ and $8m^3$ terms. However, it is possible to reduce the number of terms to $2m^2 + m$ and $\frac{2}{3}(2m^3 + 3m^2 + m)$ respectively by exploiting the symmetry of the Jacobian operators [5].

3 GENERIC NARROW–BODY AIRLINER VIRTUAL AIRCRAFT

The Generic Narrow–Body Airliner (GNBA) is a conceptual aircraft model developed by Guimarães Neto [6] for academic research purposes, conceived to be comparable to Boeing 737–500/600, Airbus A318/319, Embraer E–195 and Bombardier CS300. It was designed to operate at 38.000 ft altitude ISA and Mach 0.78. The main geometric parameters of GNBA are summarized in Table 1.

Parameter	Value	Unit
Reference wing planform area	116.0	m^2
Wing aspect ratio	9.25	–
Wing taper ratio	0.315	–
Wing span	32.756	m
Wing mean aerodynamic chord	3.862	m
Wing leading edge sweepback angle	30	deg
Equivalent wing quarter–chord sweepback angle	27.52	deg
Horizontal tail planform area	25.03	m^2
Horizontal tail aspect ratio	5.5	–
Vertical tail planform area	20.49	m^2
Vertical tail aspect ratio (root to tip)	1.7	–
Fuselage length	39.15	m
Maximum fuselage diameter	3.7	m

Table 1: GNBA Main Geometric Parameters [6].

The GNBA finite element model was created in MSC/NASTRAN [7] and consists of CBAR elements for wings, horizontal tail, vertical tail, fuselage, pylons, engine and for the structural links between the connected components. It also includes rigid bar elements used to connect the structural nodes to the lumped–mass elements. All the materials constituting the aircraft were assumed to be isotropic.

The GNBA has three levels of flexibility: Nominal, W050F050 and W025F025. For each level, the stiffness properties of the beam elements in the wing and wing–fuselage connection are multiplied by a factor σ_w and the stiffness properties of the fuselage beam elements are multiplied by a factor σ_f. Table 2 presents the value of these factors for each level of flexibility.

Configuration	σ_w	σ_f
Nominal	1.0	1.0
W050F050	0.5	0.5
W025F025	0.25	0.25

Table 2: GNBA Levels of Flexibility [6].

The elastic modes were calculated via structural dynamic model and modes up to 25 Hz were considered for modal superposition. For the W025F025 configuration, the most flexible configuration, used in the present work, has a total of 42 elastic modes. Table 3 presents some of the elastic modes and their respective frequencies for the three GNBA configurations and Fig. 1 illustrates the aircraft trimmed and the first wing and fuselage modes.

Flexible Mode	W025F025	W050F050	Nominal
First symmetric wing bending frequency [Hz]	1.07	1.50	2.13
First asymmetric wing bending frequency [Hz]	1.51	2.12	2.96
First fuselage lateral bending frequency [Hz]	2.20	3.09	4.40
First fuselage vertical bending frequency [Hz]	2.29	3.21	4.49
Symmetric engine pitching frequency [Hz]	3.47	4.45	5.53
Asymmetric engine pitching frequency [Hz]	3.54	4.77	6.21

Table 3: GNBA Flexible Modes Frequencies [6].

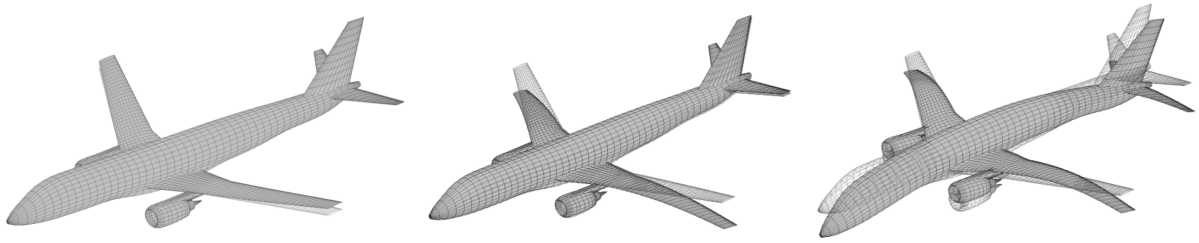

Figure 1: GNBA aircraft: trimmed, first wing bending mode and first fuselage bending mode [8].

The GNBA W025F025 implementation used in the current work, designated by FOM (Full–Order Model), is based on mean axis formulation [9] with doublet–lattice aerodynamics. The state vector contains 518 states, and is represented by

$$\boldsymbol{x} = \begin{bmatrix} V & \alpha & q & \theta & H & \beta & \phi & p & r & i_{ht} & \delta_e & \delta_a & \delta_r & T & \{\eta\} & \{\dot{\eta}\} & \{\lambda\} \end{bmatrix}^T, \tag{18}$$

where V is the flow velocity, α is the angle of attack, β is the sideslip angle, p,q and r are the angular rates, θ and ϕ are the Euler angles, H is the altitude, i_{ht} is the horizontal empennage angle, δ_e, δ_a, δ_r are the elevator, aileron and rudder deflection angles, respectively, T is the throttle, $\{\eta\}$ and $\{\dot{\eta}\}$ are the structural generalized coordinates and their time–derivatives, each of them containing 42 elements, and $\{\lambda\}$ is the aerodynamic lag vector containing 420 elements, 10 aerodynamic lags for each structural mode.

The control input vector $\boldsymbol{u}$ is defined by

$$\boldsymbol{u} = \begin{bmatrix} i_{htc} & \delta_{ec} & \delta_{ac} & \delta_{rc} & T_c \end{bmatrix}^T, \tag{19}$$

where i_{htc} is the horizontal empennage commanded angle, δ_{ec}, δ_{ac} and δ_{rc} are the elevator, aileron and rudder commanded angles respectively and T_c is the commanded thrust. More detailed information about the GNBA aircraft model can be found in reference [6].

4 THE NONLINEAR REDUCED ORDER MODEL (ROM) DESIGN

In order to evaluate the model order reduction technique [5] for real–time simulation purposes, the reduced–order model (designated by ROM) was generated from the GNBA W025F025 dynamics [6]. The ROM basis was formed by 30 pairs of left and right eigenvectors associated to the lowest frequencies eigenvalues of the full–order model (designated by FOM). Fig. 2 illustrates the map of poles for both models, FOM and ROM. The nonlinear part is composed

by the quadratic terms only, the cubic terms in the Eq. (15) were neglected, i.e., the ROM dynamics is described by

$$\dot{z}_i = \lambda_i z_i + \boldsymbol{\psi}_j^T \Big(\frac{\partial \boldsymbol{F}}{\partial u} \boldsymbol{\Delta u} + \frac{1}{2!} B_i(\boldsymbol{\Delta z}, \boldsymbol{\Delta z}) \Big). \tag{20}$$

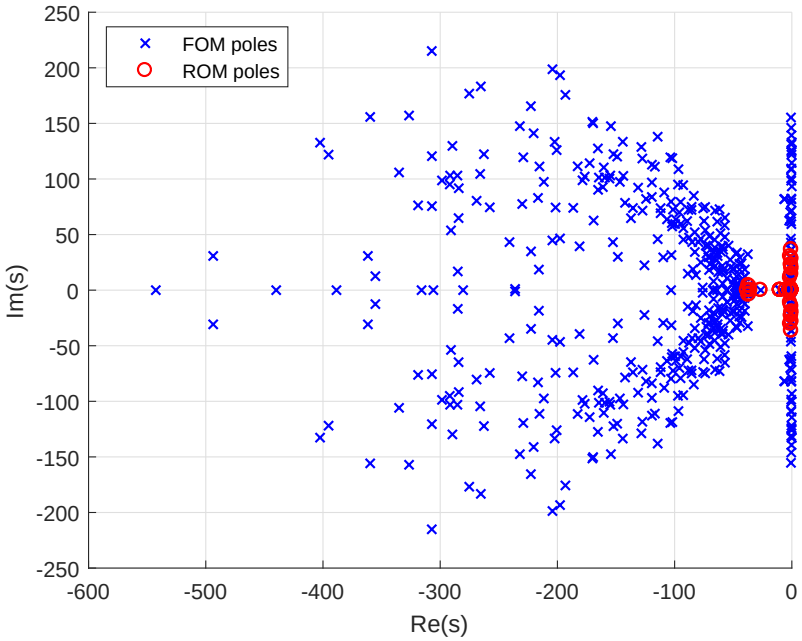

(a) Poles overview.

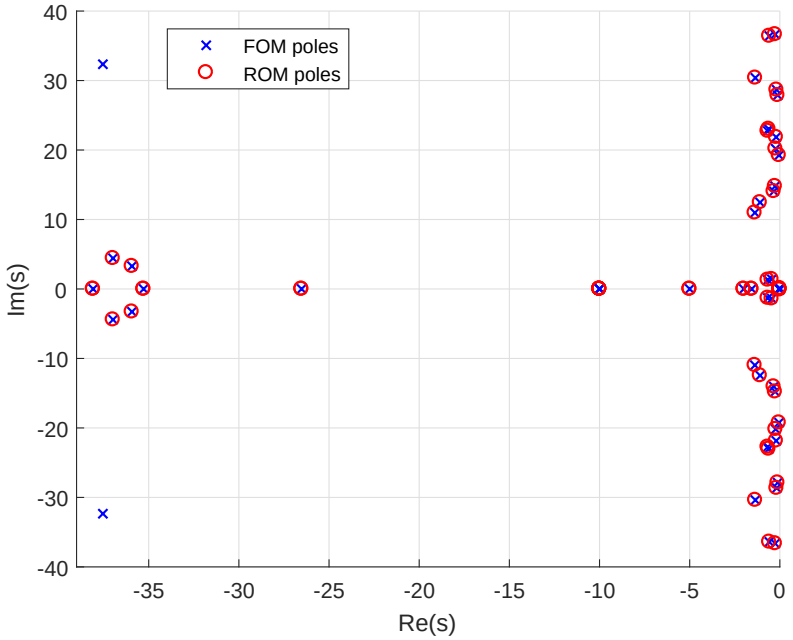

(b) Detail on low frequency poles.

Figure 2: FOM and ROM map of poles.

The ROM was implemented in MATLAB. In order to be computationally efficient, complex

arithmetic was avoided. The ROM complex coefficients were separated in real and imaginary parts and implemented as sparse matrices.

The integration algorithm chosen to perform the simulations was the MATLAB Runge–Kutta 4th–order method (ODE–4). The hardware and software configurations used to perform the simulations and to asses performance are summarized in Table 4.

Component	Specification
CPU	Intel Core i7 4510U 2.6 GHz
RAM Memory	8,00 GB
Operational System	Windows 10 Home
Framework	MATLAB R2017a

Table 4: Hardware and Software Specification.

5 RESULTS

This section contains results obtained via simulation for specific test cases designed to explore nonlinearities of the aircraft model. The ROM is compared with three different approaches: the nonlinear FOM which represents the dynamics that we would like to reproduce, the linear FOM which is a fast alternative for real–time simulations and the rigid–body with quasi–static aeroelastic correction [6] which consists in a rigid–body approach with modified aerodynamic coefficients such that the poles relative to rigid–body dynamics match with the corresponding poles in the flexible model.

Velocity and altitude signals were evaluated in the aircraft center of gravity while the angles and angular rates were evaluated in the aircraft cockpit, i.e. they include rigid–body and flexibility effects.

5.1 Response to a rudder doublet

This test case demonstrates the limitation of the linearized model in reproducing the aircraft longitudinal behavior due to a rudder command. A 10 degree doublet command was applied to the rudder (Fig. 3), the longitudinal and lateral responses are presented in the Figs. 4 and 5, respectively.

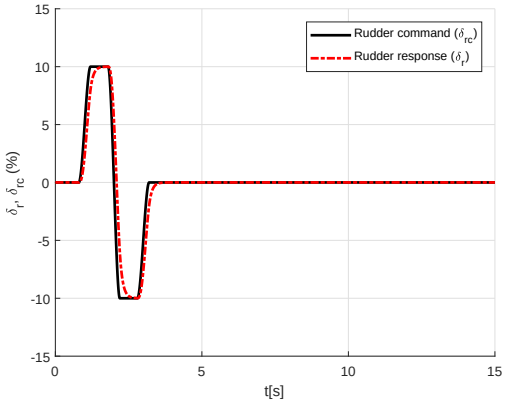

Figure 3: Rudder 10 degree doublet excitation.

Although the three approximations could represent the lateral–directional dynamics behavior well, it is worth note that the linear FOM longitudinal response remains close to the initial conditions during the entire flight while the nonlinear FOM indicates that the aircraft is actually performing a coupled longitudinal motion. Both, ROM and rigid–body approximation, were able to reproduce the longitudinal dynamics. However, the ROM achieved a more accurate response.

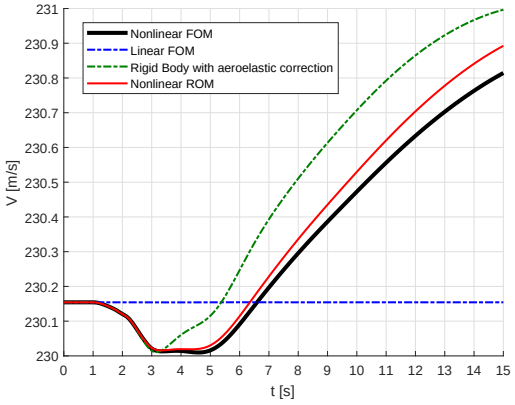

(a) Velocity.

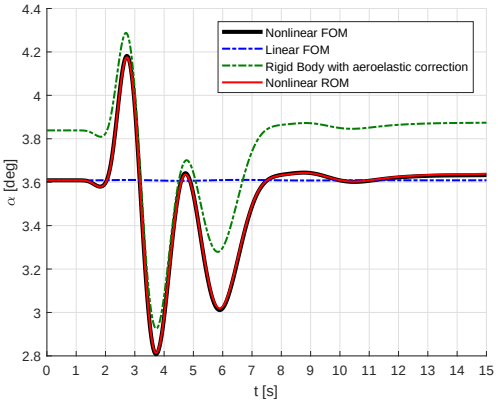

(b) Angle of Attack.

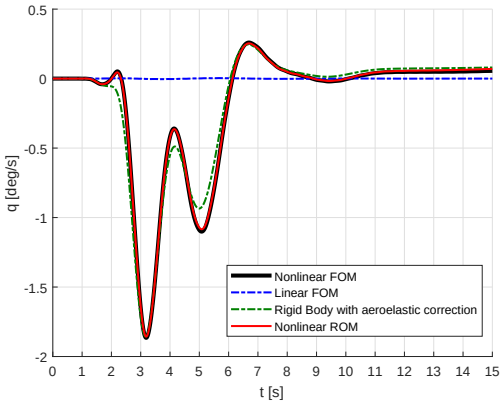

(c) Pitch rate.

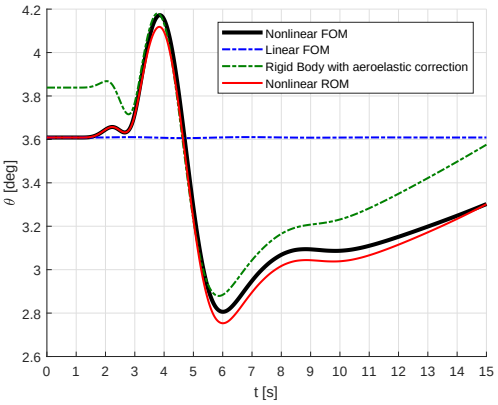

(d) Pitch angle.

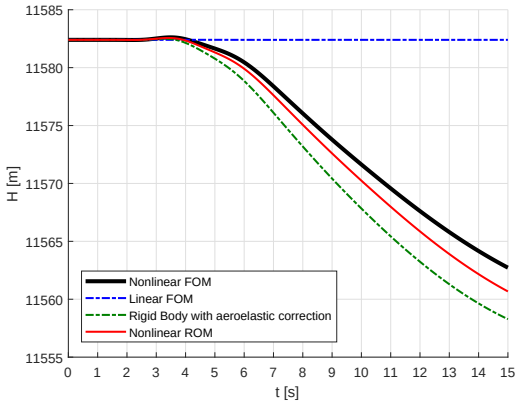

(e) Altitude.

Figure 4: Longitudinal response due to a 10 degree rudder doublet.

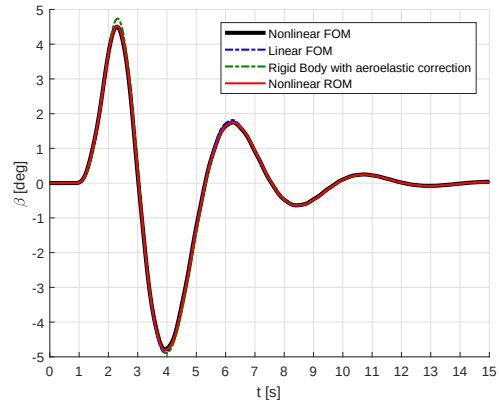

(a) Sideslip angle.

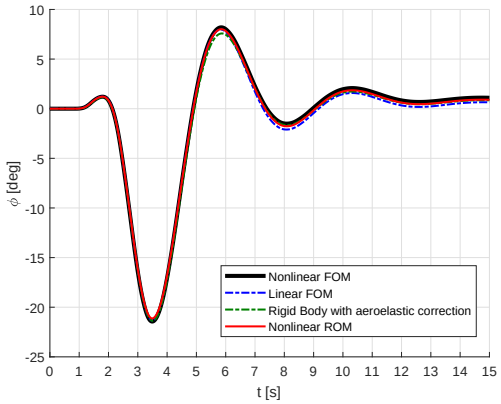

(b) Bank angle.

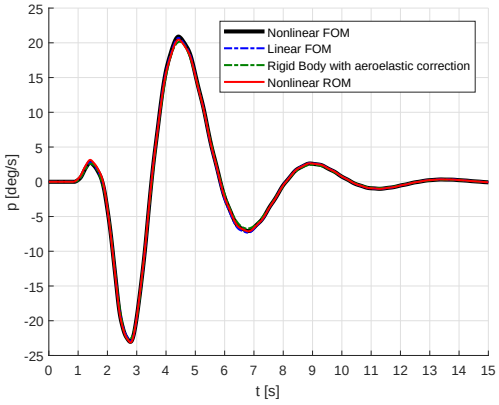

(c) Roll rate.

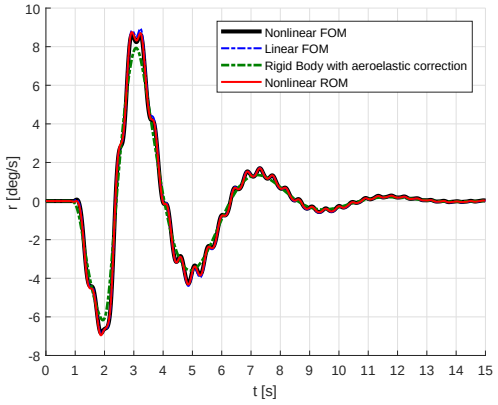

(d) Yaw rate.

Figure 5: Lateral response due to a 10 degree rudder doublet.

5.2 Response to an aileron and elevator doublet

This test case demonstrates the aircraft longitudinal (Fig. 7) and lateral responses (Fig. 8) due to a 10 degree simultaneous aileron and elevator doublet (Fig. 6).

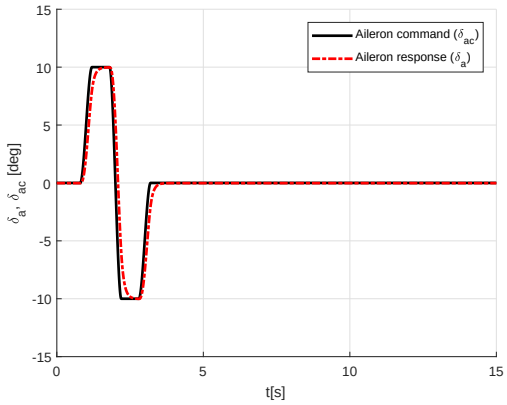

(a) Aileron excitation.

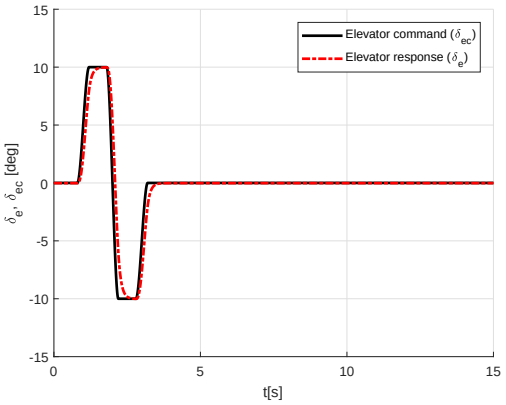

(b) Elevator excitation.

Figure 6: Aileron and elevator 10 degree doublet excitation.

In general, the ROM fits the FOM response better than the other approaches. Note that rigid–

body approach can not represent vibrations produced by the elastic deformation, as shown in Fig. 7(c) and in Fig. 8(d). Additionally, the rigid–body approach could not represent the altitude response accurately, as shown in Fig. 7(e). On the other hand, the linear approach had problems representing the bank angle response, as shown in Fig. 8(b), while the proposed ROM could represent all the responses accurately.

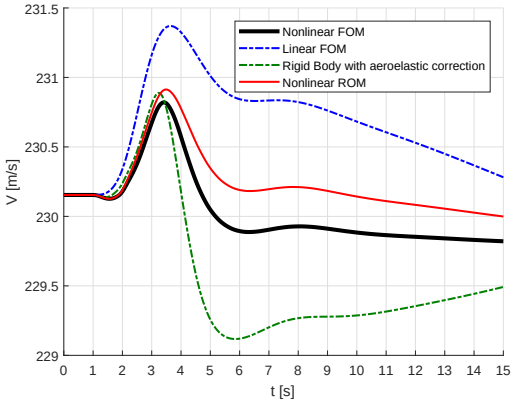

(a) Velocity.

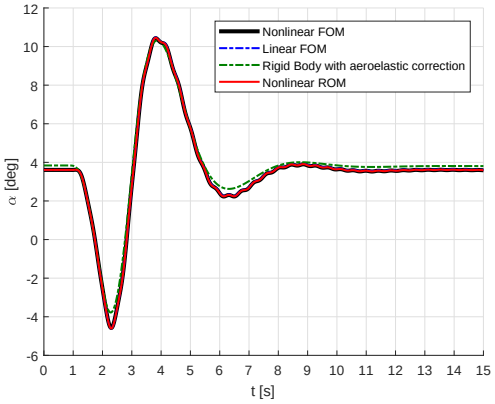

(b) Angle of Attack.

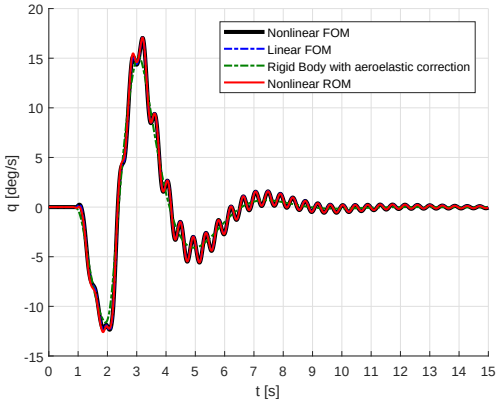

(c) Pitch rate.

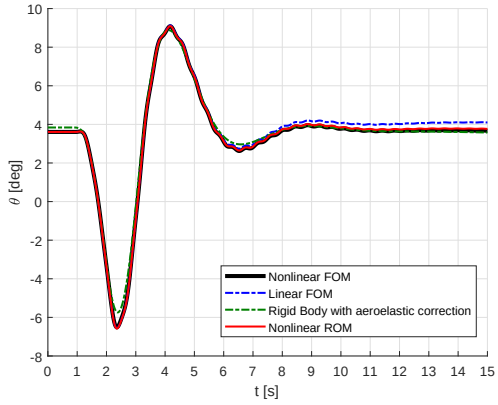

(d) Pitch angle.

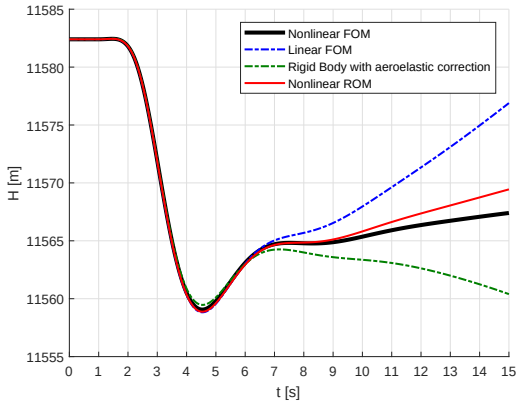

(e) Altitude.

Figure 7: Longitudinal response due to a simultaneous 10 degree aileron and elevator doublet.

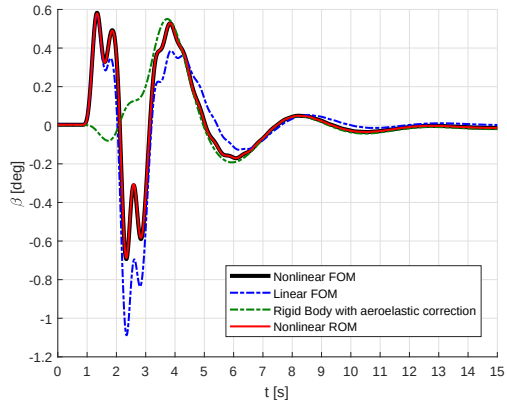

(a) Sideslip angle.

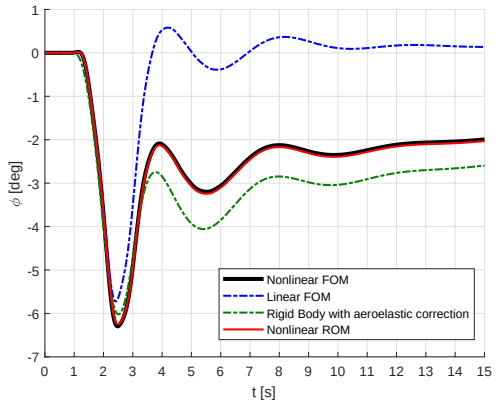

(b) Bank angle.

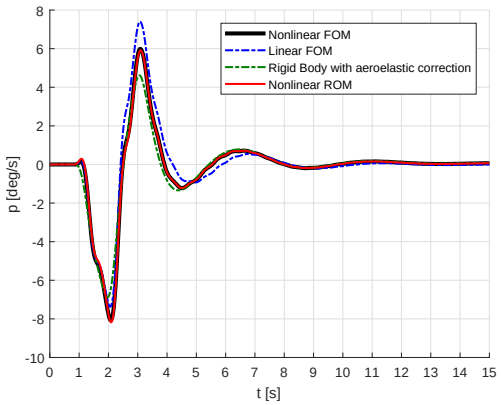

(c) Roll rate.

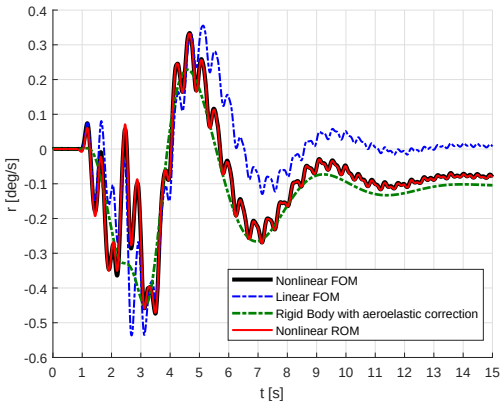

(d) Yaw rate.

Figure 8: Lateral response due to a simultaneous 10 degree aileron and elevator doublet.

5.3 Method Limitations

The model order reduction technique [5] is based on Taylor series expansion around an equilibrium point which means the approximation is local. As the operation point moves away from the equilibrium, the ROM approximation loses accuracy.

To illustrate the effect of this limitation, Fig. 9 shows the pitch angle and altitude responses due to a step excitation that increases the thrust by 20% of its equilibrium value while Fig. 10 shows the responses of the same variable for an increase of 50%. Note that for the second case, the ROM approximation becomes slightly worse than the first one.

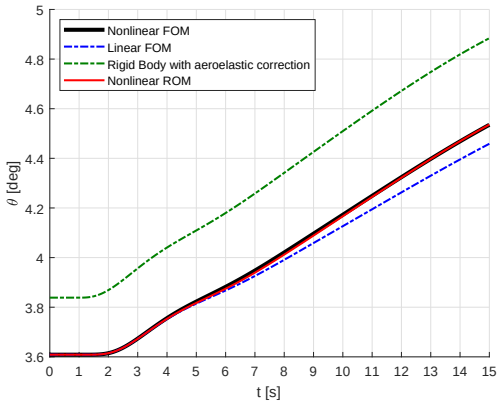

(a) Pitch angle.

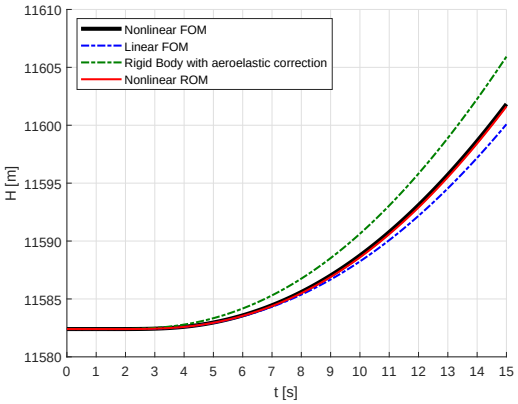

(b) Altitude.

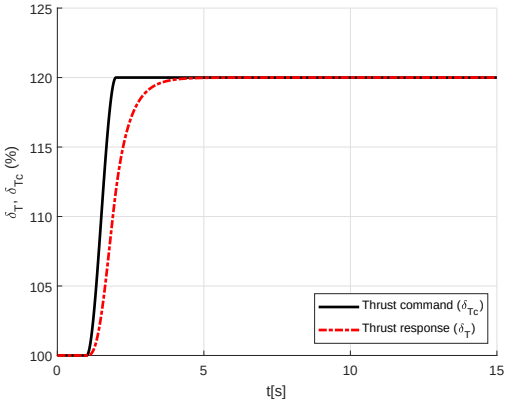

(c) Thrust.

Figure 9: Pitch angle and altitude responses due to a thrust step of 20% of the trimmmed thrust $(T_0 = 29,866N)$.

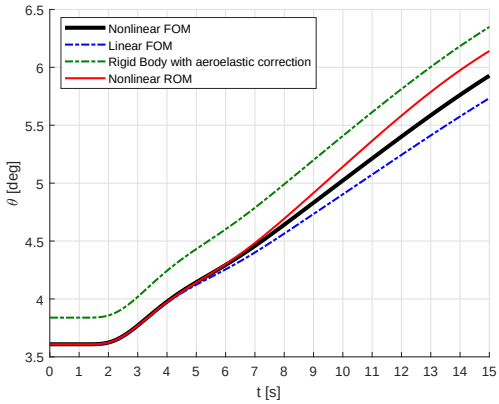

(a) Pitch angle.

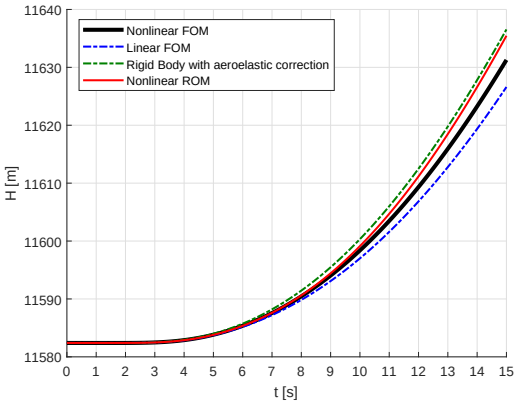

(b) Altitude.

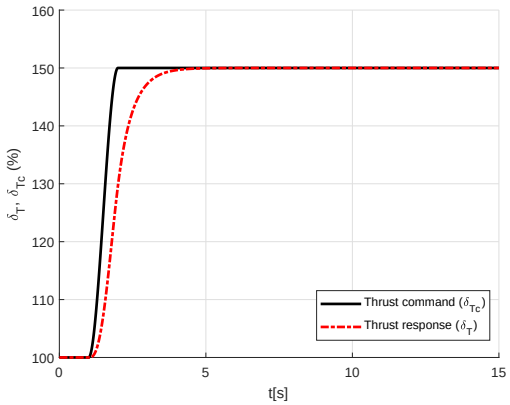

(c) Thrust.

Figure 10: Pitch angle and altitude responses due to a thrust step of 50% of the trimmmed thrust $(T_0 = 29,866N)$.

5.4 Assessment of Computational Cost

The objective of this subsection is to demonstrate the performance gain of the ROM relatively to the FOM. This gain is mainly achieved by the simpler polynomial ROM formulation, the reduced number of equations and state variables. Additionally, the increase of the simulation time step size necessary for convergence also contributes to a even lower average simulation time. Since the ROM is formed by low frequency modes only (Fig. 2), there is no need to use small time step sizes as in the FOM.

The timing measurements were made in the computer described in Table 4. Five 15–seconds flight simulations were performed for each case. Table 5 presents the average simulation time and the respective standard deviation for each case.

Model	Time step (ms)	Average simulation time (s)	Standard deviation (s)
FOM	5	892.091	3.822
ROM	5	8.555	0.131
ROM	10	4.453	0.150

Table 5: Comparison between FOM and ROM simulation time of a 15–seconds flight.

Comparing the first two lines of Table 5, where ROM and FOM were simulated with the same time step, it is observed a gain of 104.2 times in the simulation time due to the smaller number

of equations and simpler polynomial formulation. When we consider the time step increase, the total simulation time gain is equal to 200.33 times.

6 CONCLUSION

In this paper, we applied a nonlinear model order reduction technique to an aircraft of moderate flexibility for real–time simulation purposes. Test cases were presented to compare the approximation made by the reduced–order model with other traditional fast simulation models. Furthermore, a comparison between the reduced–order model and the full–order model simulation time was made showing significant performance improvement.

Results showed that the reduced–order model was able to approximate in real–time the full–order model dynamics around the equilibrium point better than the linearized model and the rigid–body model with aeroelastic correction.

The overall assessment is that the technique is promising for real–time simulations of flexible aircraft.

Future work will focus on the application of the reduced order model to a highly flexible aircraft and on the control synthesis design for maneuver and load alleviation.

7 REFERENCES

[1] Kaden, A., Boche, B., and Luckner, R. (2013). Hardware-in-the-loop flight simulator - an essential part in the development process for the automatic flight control system of a utility aircraft. *Advances in Aerospace Guidance, Navigation and Control*, Springer, Berlin, pp 585–601.

[2] Waszniowski, L., Hanzálek, Z., and Doubrava, J. (2011). Aicraft control system validation via hardware-in-the-loop simulation. *Journal of Aircraft*, 48(4), 1466–1468.

[3] González, P., Boschetti, P., Cárdenas, E., et al. (2010). Evaluation of the flying qualities of a half-scale unmanned airplane via flight simulation. *48th AIAA Aerospace Sciences Meeting Including the New Horizons Forum and Aerospace Exposition*, AIAA Paper 2010–298.

[4] Kish, B., Leggett, D., Nguyen, B., et al. (1996). Concepts for detecting pilot-induced oscillation using manned simulation. *21st Atmospheric Flight Mechanics Conference, Guidance, Navigation, and Control and Co-located Conferences*, pp. 559–568.

[5] Da Ronch, A., Badcock, K., Wang, Y., et al. (2012). Nonlinear model reduction for flexible aircraft control design. *AIAA Atmospheric Flight Mechanincs Conference*, AIAA Paper 2012–4404.

[6] Guimarães Neto, A. (2014). *Flight Dynamics of Flexible Aircraft Using General Body Axes: a Theoretical and Computational Study, PhD Thesis*. Instituto Tecnológico de Aeronáutica.

[7] MSC Software (2005). *MSC Nastran 2005r3 quick reference guide*. Newport Beach.

[8] Silvestre, F., Guimarães Neto, A., Bertolin, R., et al. (2017). Aircraft control based on flexible aircraft dynamics. *Journal of Aircraft*, 54(1), 262–271.

[9] Waszak, M. and Schmidt, D. (1988). Flight dynamics of aeroelastic vehicles. *Journal of Aircraft*, 25(6), pp.563–571.

COPYRIGHT STATEMENT